Japan Architectural Review
Open Access

Architectural Institute of Japan

Translated Paper

Shaking table tests on spherical sliding bearings taking eccentricity and uplift into account

Toru Takeuchi,[1] Hideji Nakamura,[2] Masakaze Uchida,[3] Michiyasu Yoshida[4] and Ryota Matsui[5]

[1]Department of Architecture and Building Engineering, Tokyo Institute of Technology, Tokyo, Japan; [2]Nakamura Structural Laboratory, Tokyo, Japan; [3]Chiyoda Corporation, Yokohama, Japan; [4]Structural Design Plus-One, Tokyo, Japan; [5]Department of Socio-Environmental Engineering, Hokkaido University, Sapporo, Japan

Correspondence
Toru Takeuchi, Department of Architecture and Building Engineering, Tokyo Institute of Technology, Tokyo, Japan.
Email: takeuchi.t.ab@m.titech.ac.jp

The Japanese version of this paper was published in Volume 80 Number 715, pages 1385–1392, https://doi.org/10.3130/aijs.80.1385 of *Journal of Structural and Construction Engineering (Transactions of AIJ)*. The authors have obtained permission for secondary publication of the English version in another journal from the Editor of the *Journal of Structural and Construction Engineering (Transactions of AIJ)*. This paper is based on the translation of the Japanese version with some slight modifications.

Received November 20, 2018; Accepted February 1, 2019

doi: 10.1002/2475-8876.12080

Abstract

Although rubber bearings are popular in Japan as seismic isolation bearings, spherical sliding bearings (SSBs) or friction pendulum bearings are widely used in many countries, including the U.S. In this study, shake table tests on a braced frame supported by SSBs are carried out, and their dependence on pressure and velocity is investigated. Tests under eccentric dead loads and uplift conditions are also conducted to capture their performance. Analytical models that consider pressure and velocity dependence are proposed, and their validity against the experimental results is discussed.

Keywords
eccentricity, friction pendulum bearing, seismic isolation, shake table test, uplift

1. Introduction

Although laminated rubber bearings are still principally used for seismically isolated buildings in Japan, spherical sliding bearings (SSBs) or friction pendulum bearing (FPBs) have been employed for practical use in many isolated buildings in the U.S. and other countries since the early 1990s. A SSB is generally composed of a slider with a smooth polytetrafluoroethylene (PTFE) surface and concave plates with a spherical surface covered with stainless steel or other materials. It features pendulum motion and hysteresis-damping mechanisms owing to frictional force. It can also easily realize a long natural period by controlling the curvature of the concave plates. Compared with the single type of bearings in which the slider is fixed on one side plate and on the slides on the other spherical surfaces,[1] the double type of bearings in which independent sliders are arranged between the upper and lower concave-plate spherical surfaces[2] has an allowable amplitude close to the diameter of the concave plate. This is most popularly used owing to its deformability characteristic (Figure 1). The SSB can determine its natural period irrespective of the supporting weight and can adjust the maximum deformation because of the concave-plate curvature, which is difficult for laminated rubber bearings, especially in lightweight structures. Therefore, SSBs are suitable for seismically isolated roofs or lightweight housings, which have been employed to support the roof structures of airports[3] or the terminal buildings themselves for seismic isolation.[4]

Fundamental experiments on SSBs have been conducted in Japan since the 1990s,[5] and shake table tests that assumed houses for nuclear power plants have been carried out in recent years.[6] However, the following problems have been pointed out.

1. Because the frictional force changes along the vertical force, a risk is present in that the upper structure could twist when the frictional force is unevenly distributed in the bearing portion where the weight is eccentric or the axial force varies.
2. When the upper part of the bearings is uplifted, the displacement of the sliders at these positions are difficult to predict because it is unrestrained.

In the current research, therefore, we perform shake table tests of an SSB supporting frame under eccentric and uplift conditions and confirm the response characteristics of the SSB under abovementioned problems (1) and (2). Generally, PTFE sliding bearings are known to depend on velocity and surface pressure.[7,8] First, dynamic loading tests are carried out by changing the seismic input and surface pressure, and the velocity and bearing pressure dependence of the frictional force of

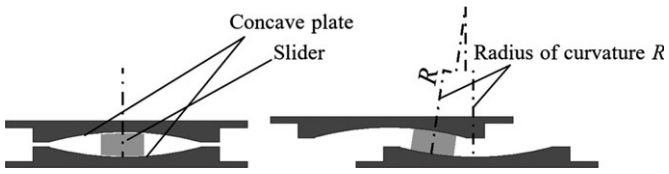

Figure 1. Conceptual diagram of the SSB

the SSB is identified. Then, shake table tests that employ eccentric weight and uplifting are performed, and the vibration response characteristics concerning problems (1) and (2) are investigated. Furthermore, a dynamic analysis model is proposed by combining the bilinear history model using a dashpot. The experimental results are simulated using the proposed dynamic model, which confirms its applicability.

2. Dynamic loading tests of SSBs

To investigate the abovementioned problems, a reduced-scale test frame supported by SSBs are constructed as described below, and dynamic loading tests are initially carried out.

2.1 Specimen overview

Figure 2 shows the test frame. The specimen is a steel frame with a single span in two directions (1000 × 1000 × 600 mm), and detachable chevron steel braces are added to the four perimeter planes to increase the horizontal stiffness of the frame. Furthermore, the vertical forces are varied by loading a number of counter weights (78 kg per piece) at the top of the column.

Figure 3 shows the SSB used in this experiment. The standard friction coefficient at a velocity of 400 mm/s and reference surface pressure (60 N/mm^2) is set to 0.047, similar to that of a general-purpose size [9]. The slider diameter ϕ = 30 mm, and the radius of curvature of the concave plate surface R = 2500 mm. The natural period is approximately 4.5 seconds, as obtained from Equation (1), where g is the gravitational acceleration.

$$T = 2\pi\sqrt{\frac{2R}{g}} \tag{1}$$

2.2 Dynamic characteristics of SSB

First, dynamic-loading tests using a constant-amplitude wave input are performed on the specimen frame attached to a fixed test frame via a load cell, and the characteristics of the SSB friction coefficient are investigated. We also confirm the validity of the evaluation of the frame shear force from the axial force of the perimeter braces and the bending-moment distribution of the columns in the specimen frame, which will be used later in the shake table tests. The setup diagram is shown in Figure 4. The total weight of the test frame is 18.62 kN

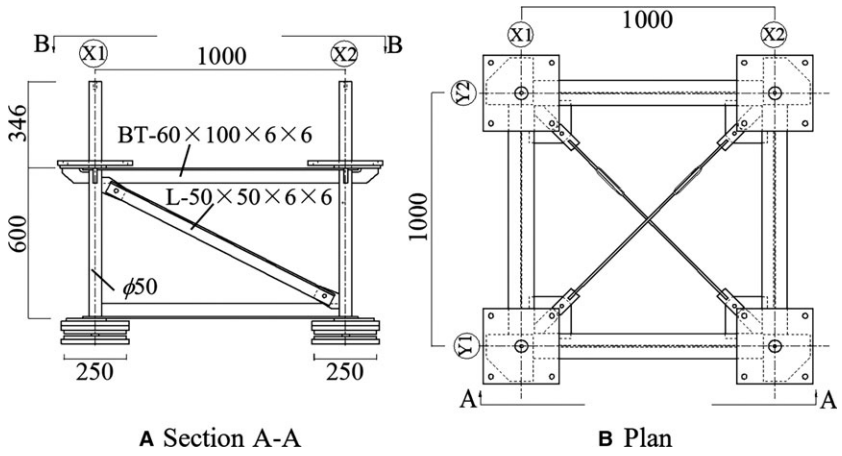

Figure 2. Test frame (mm)

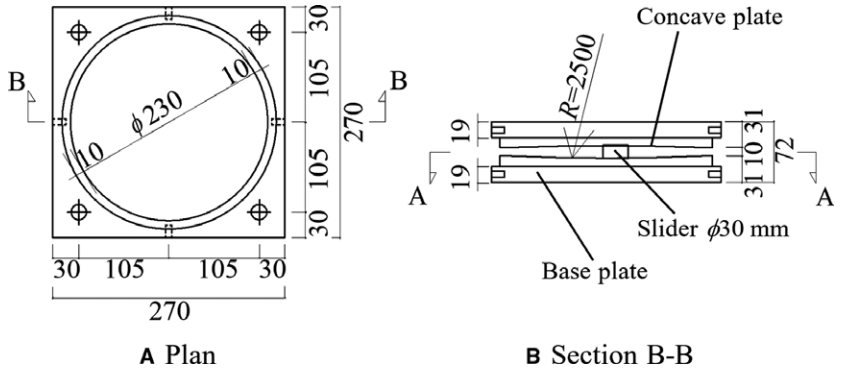

Figure 3. Composition of the SSB (mm)

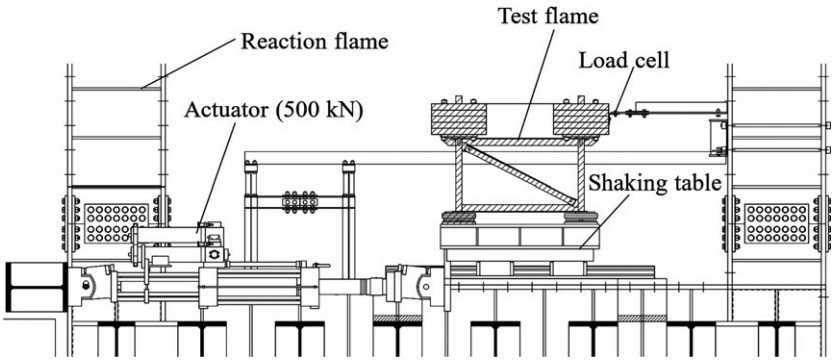

Figure 4. Setup of dynamic-loading test

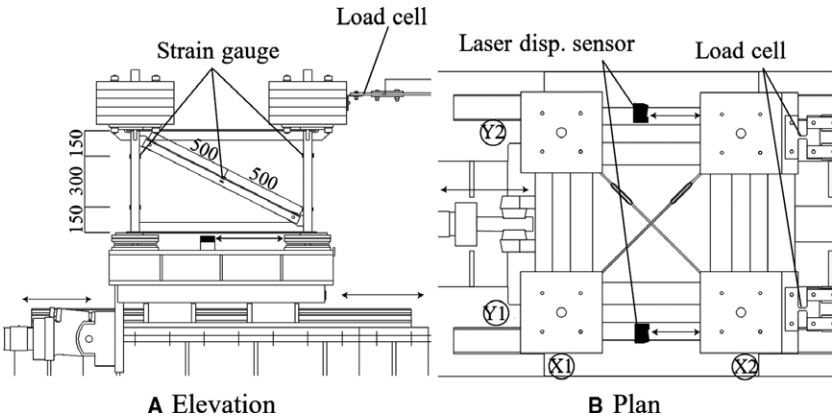

Figure 5. Measurement instrumentation

including the five steel plates at the top of each column used for dead load.

Figure 5 shows the instrumentation positions. The upper concave-plate displacement of the SSB with respect to the shake table is measured using a laser displacement meter. Strain gauges are attached to the columns and braces to measure the shear forces of the columns and axial forces of the braces. We consider the sum of the horizontal components as the frame shear force. Table 1 lists the test matrix. The loading is controlled by the displacement, and triangular and sine waves are input under varying frequencies. The ratio between horizontal load F and total weight W of the specimen is defined as equivalent friction coefficient μ_{eq} and is expressed as Equation (2).

$$\mu_{eq} = F/W \tag{2}$$

Figure 6 shows a comparison of the time history of the shear force evaluated from the strain gauges and the load-cell reaction force. Both shear forces agree well, and we determine that the frame shear force in the shake table experiment can be evaluated using the strain gauges. Figure 7 shows the equivalent friction coefficient-displacement relationship. The horizontal axis represents the averaged displacement obtained by the displacement meters (LVDTs) shown in Figure 5B. The equivalent friction coefficient is distributed around 0.1, which is higher than the reference friction coefficient. This result is considered as the effect of the smaller vertical pressure of 6.6 N/mm^2, which is approximately 1/10 times the reference pressure. Figures 7C and D show that the equivalent friction coefficient varies because of the difference in the velocity even if the frequencies are the same. In addition, Figure 7A and B show that when the sign of the velocity changes, the equivalent friction coefficient increases for a triangular wave input, which is considered to be owing to the influence of inertial forces. As stated earlier, SSB depends on the velocity and surface pressure, similar to a general PTFE sliding bearing. Figures 8 and 9 show the relationships of the equivalent friction coefficients to velocity and surface pressure, respectively. These coefficients are obtained from the loading protocols, numbers 1-12 listed in Table 1, and the specimens in Reference.[9]

Table 1. Dynamic-loading tests matrix

No.	Amplitude (mm)	PGV (mm/s)	Frequency (Hz)	Shape	Cycles
1	180	23	0.02	Sine	5
2		22	0.03	Triangle	
3		102	0.09	Sine	
4		101	0.14	Triangle	
5		204	0.18	Sine	
6		202	0.28	Triangle	
7		396	0.35	Sine	
8		403	0.56	Triangle	
9	20	40	0.5	Sine	
10	50	100	0.5		
11	100	200	0.5		
12	100	-	0.2-0.5	Sine	-

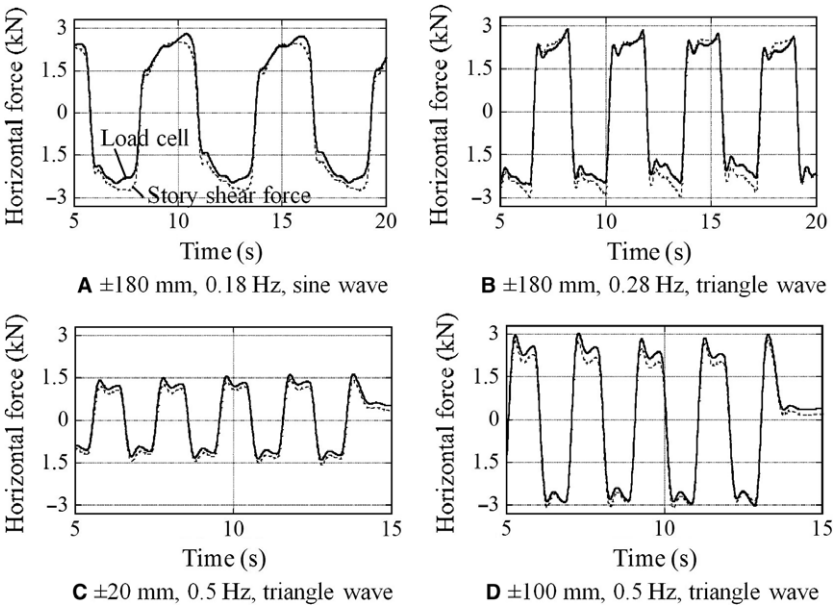

Figure 6. Time history of horizontal force (dynamic-loading test)

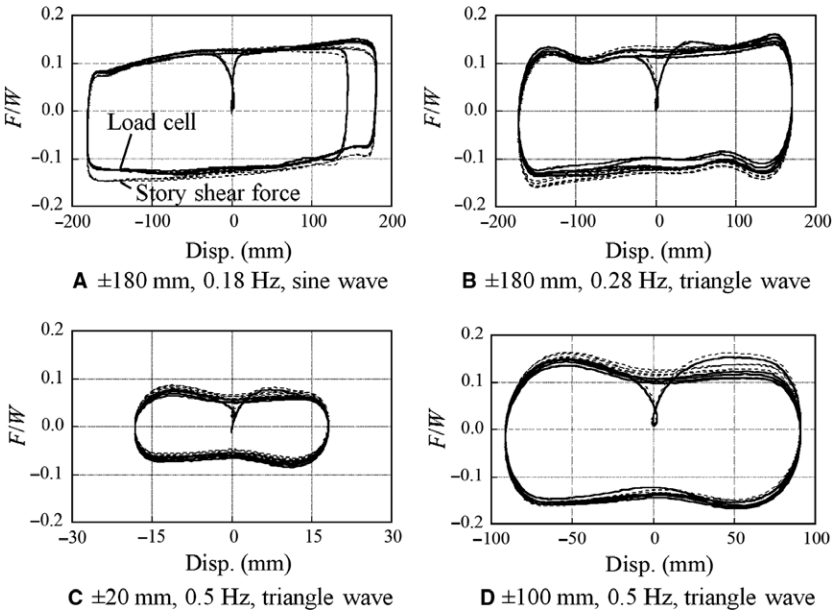

Figure 7. F/W–displacement relationships (dynamic-loading test)

The velocity is defined at the upper part of the SSB, similar to that in Ref. [9]. The equivalent friction coefficient is estimated from the positive *Y*-axis intercept value in the third cycle, whereas the entire cycle after the third cycle is used for load no. 12. Figure 9 shows that the equivalent friction coefficient converges to approximately 0.03 in the case of high surface pressure, whereas it increases to double the value under low surface pressure. Figure 8 shows that the velocity dependence also increases under low surface pressure.

3. Shake table tests of SSB

Next, the load cell with the connector is removed and shake table tests are carried out to investigate the response characteristics of the SSB under weight eccentricities and uplifting.

3.1 Shake table tests with evenly distributed weight

First, shake table tests are carried out where five weights are evenly loaded on each column. Figure 10 shows the setup of the evenly loaded specimen. Similar to the dynamic vibration test, the shear force from the strain gauges and the horizontal relative displacement of the SSB are measured by the displacement meters. The vertical displacement of the SSB is also measured at (X1, Y1), as shown in Figure 5. Table 2 lists the test matrix. The seismic wave is set at a maximum velocity of 500 mm/s.

Figure 11 shows the time history of the acceleration and horizontal equivalent friction coefficient-displacement

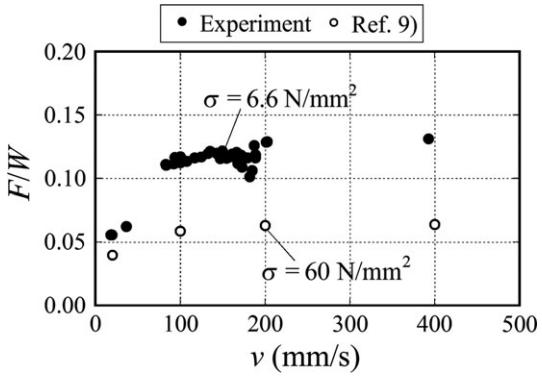

Figure 8. F/W–velocity relationship

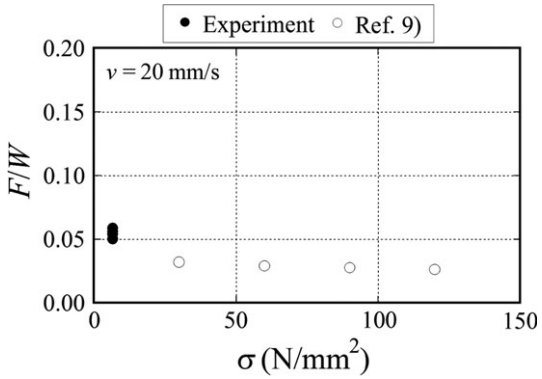

Figure 9. F/W–pressure relationships

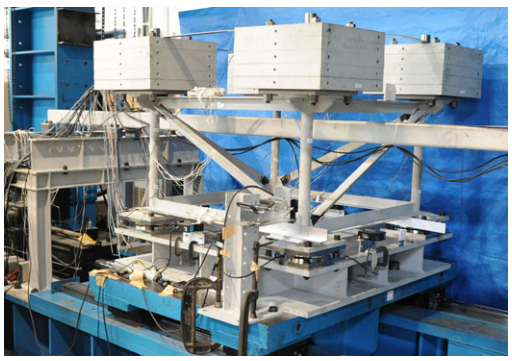

Figure 10. Setup of shake table test (evenly distributed load)

relationship under protocol no.13 (sine wave; amplitude = 30 mm) at a frequency of 1.3 Hz. Figure 11A shows that the acceleration response of the specimen frame is suppressed to approximately 1500 mm/s^2, which is equivalent to the input level. The SSB does not slide under a maximum input acceleration of less than 1500 mm/s^2, and the shake table and specimen frame move together. Figure 11B shows that the equivalent friction coefficient at maximum velocity is approximately from 0.11 to 0.13 and the velocity at this point is approximately 250 mm/s, which is identical to the relationship between the equivalent friction coefficient and velocity shown in Figure 8. In addition, the hysteresis shape becomes round compared with that shown in Figure 7, which shows the effect of the velocity dependence of the SSB, although it is partially

Table 2. Shake table tests matrix

No.	Amplitude (mm)	Frequency (Hz)	Shape
13	30	0.5-2.0	Sine
14	50	0.5-1.0	

No.	Ground motions	Scale factor
15	El Centro NS (1940)	140%
16	JMA Kobe NS (1995)	50%
17	Hachinohe NS (1968)	140%

due to the data sampling frequency. Figure 12 shows the equivalent friction coefficient-horizontal displacement relationship in the seismic wave input. The figure indicates that the maximum equivalent friction coefficient is stable up to approximately 0.14 at the maximum. Figure 13 shows the horizontal-displacement time history. Some residual displacements remain in all seismic waves because the weight of the specimen frame is lighter and the equivalent friction coefficient of the sliding is higher owing to the low pressure, and obtaining a sufficient self-centering force is difficult. Compared with a pulsed JMA Kobe wave, the residual displacement under the other two seismic waves is less significant. Even if the residual displacement remains after an earthquake, it is resolved and self-centered under several after shakes.

3.2 Shake table tests with eccentric weight

Using the same setup presented in the previous section, shake table tests using eccentric weights are carried out in which four counter weights in the Y2 plane are removed. The weight ratio of Y1/Y2 is 3:1. Figure 14 shows the test setup. The measurement and loading specifications are the same as those in the previous tests. To evaluate the torsional response, twist angle ψ is defined as shown in Figure 15. Torsional angle ψ is defined by Equation (3) using bearing horizontal displacement δ_i and distance between the measurement points L.

$$\psi = (\delta_1 - \delta_2)/L \tag{3}$$

Figure 16 shows the equivalent friction coefficient – horizontal displacement relationship of the seismic-wave input compared with the evenly distributed weight test results. Generally, the results obtained from the eccentric-weight tests are identical to those of the even-weight tests. Thus, we can see that the response characteristics of the SSB under eccentric loading are similar as those under evenly distributed weighted conditions with maximum 20% errors in displacements. Figure 17 shows the torsional-angle time history compared with that for the evenly distributed weight tests. In the eccentric-weight tests, the twist angle is 0.5% rad, which is as small as the twist in the uniform weight believed to be caused by misalignment of the SSBs as will be described later. The difference is small.

3.3 Shake table tests with uplift

Finally, the specimen frame is rotated by 45° with respect to the input direction, and shake table tests accompanied by SSB uplift are performed. Two types of tests are compared: the first uplifts the corner bearing by unloading the corner-column weight and the second does not uplift the corner bearing by evenly loading the four columns. Figure 18 shows the setup for the uplifting tests. As shown in Figure 19, only two braces are attached to the frame, and the uplift of the column near

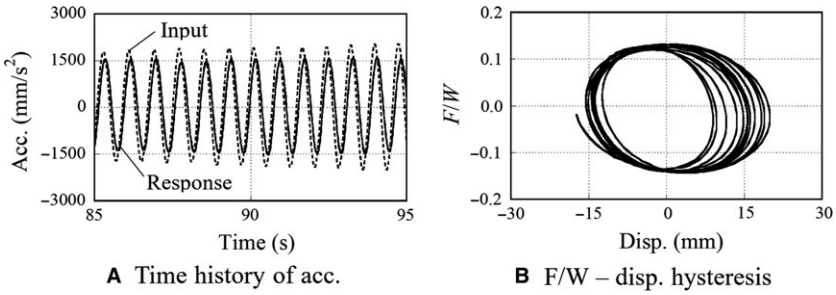

Figure 11. Response of sweep sine wave (±30 mm; 1.3 Hz)

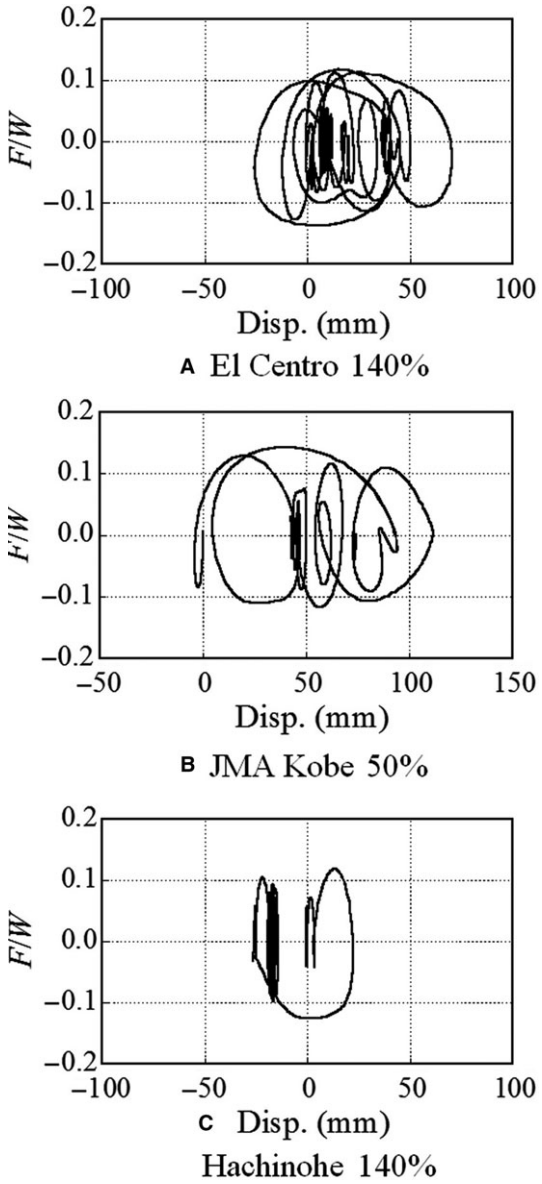

Figure 12. F/W–Horizontal displacement relationships

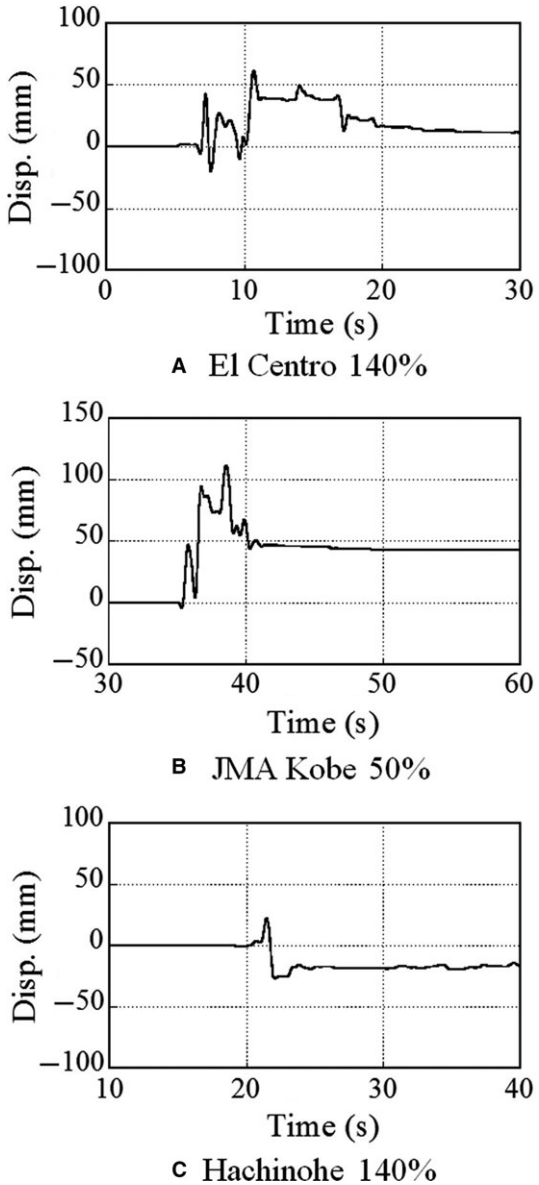

Figure 13. Horizontal displacement time histories

the braces is induced along the horizontal response. Figure 20 shows the uplifted corner-column position and removed brace position, together with a measurement diagram. The measurement equipment is the same as that in the even-weight tests, and the seismic waves listed in Table 2 are employed.

Figure 21 shows the obtained equivalent friction coefficient-horizontal displacement relationship. The displacement along the horizontal axis represents the average value of the laser displacement sensors shown in Figure 20. When compared with the uniform and corner-removal loading, maximum displacement

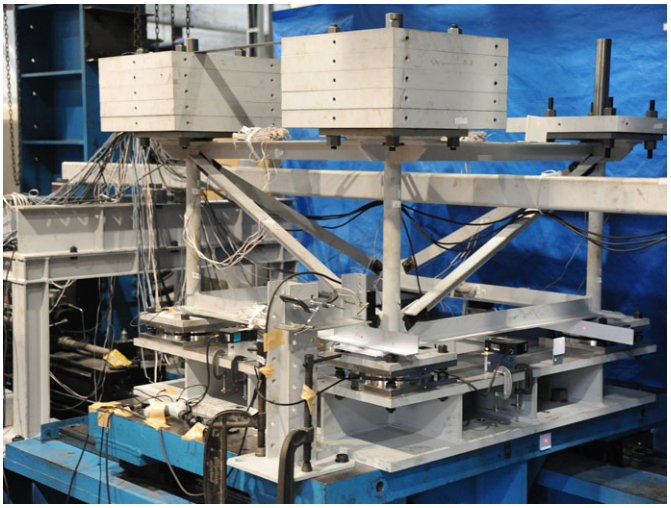

Figure 14. Setup of shake table test (eccentric load)

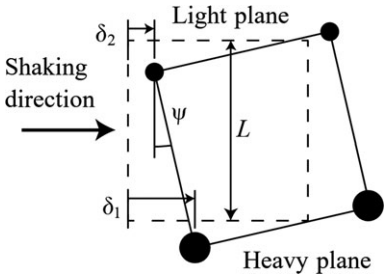

Figure 15. Horizontal twist

discrepancies of approximately 40% and 10% of the equivalent friction coefficient are observed in the Hachinohe waves. However, both show similar hysteresis curves and phases.

Next, the vertical displacement at point XY1 in Figure 20 is confirmed. In this experiment, a case exists where the lowest point of the concave plate starts from the position that deviates from the center because of horizontal angle error θ of the SSB attachment, as shown in Figure 22. The displacement error is approximately from 25 to 50 mm, which corresponds to θ of approximately 1/200 to 1/100 rad. In the vertical-displacement graph in the following section, the vertical displacement of the upper concave plate is calculated by correcting this error.

Figure 23 shows the vertical displacement orbit obtained from the test results. The corrected calculated value corresponds well with the uniform-loading test results. On the other hand, the corner-removal loading results show a larger vertical displacement than the evenly loaded tests. The difference between the measured vertical displacement and corrected calculated value is evaluated as the estimated uplifting displacement. Figure 24 shows the time history of the estimated uplifting displacement, which shows that 0.4-0.8 mm of uplifting occurs in each seismic wave. We also confirm the vertical residual displacement. Using video and a fiber-scope, we observe that the idle run of the upper plate occurs without capturing the slider, as shown in Figure 25. Here, we consider that the slider deviates from the original position, and a residual vertical displacement remains afterward. On the other hand, Figure 21 shows that the influence of uplifting is insignificant with respect to the horizontal response and effects of seismic isolation. We also observe that the vertical residual

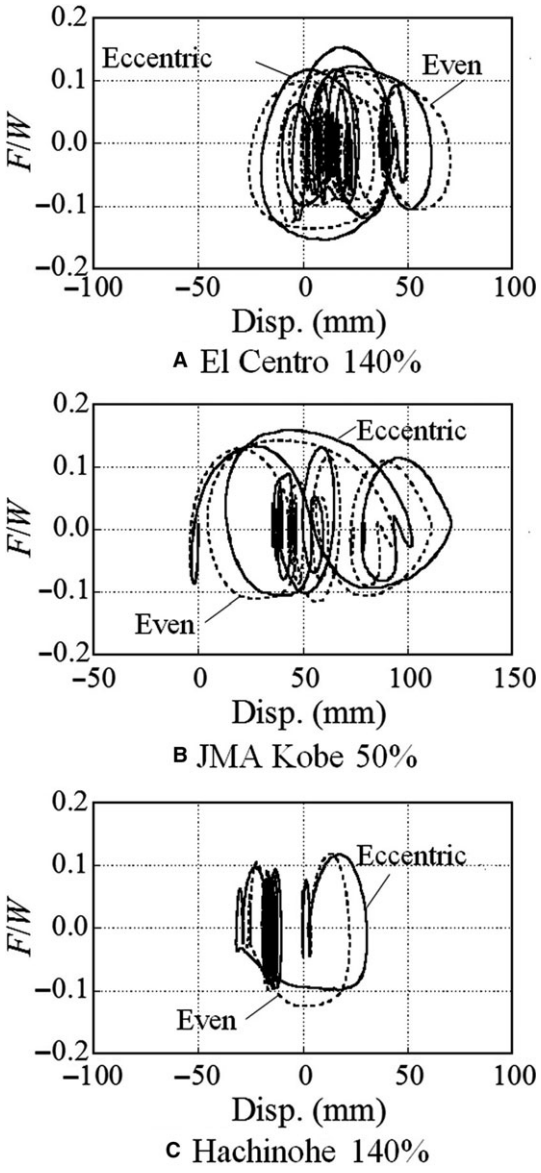

Figure 16. F/W–Horizontal displacement relationships

displacement is resolved by the return of the slider to the original position because of subsequent excitation.

4. Proposal for analytical model and response

In this section, according to the experimental results presented in the previous sections, a dynamic analytical model of an SSB that considers the friction coefficient velocity and bearing pressure dependence is proposed. As a dynamic model, we propose a model that combines the viscous elements, in addition to a bilinear elasto-plastic element,[10] which has generally been used for friction models in time-history analyses.

4.1 Composition of SSB dynamic model

In the SSB, the friction coefficient expressed by Equation (4) was proposed by Nakamura et al.[9] The underlined part at the right side shows the surface-pressure dependence, and the double-underlined part shows the velocity dependence.

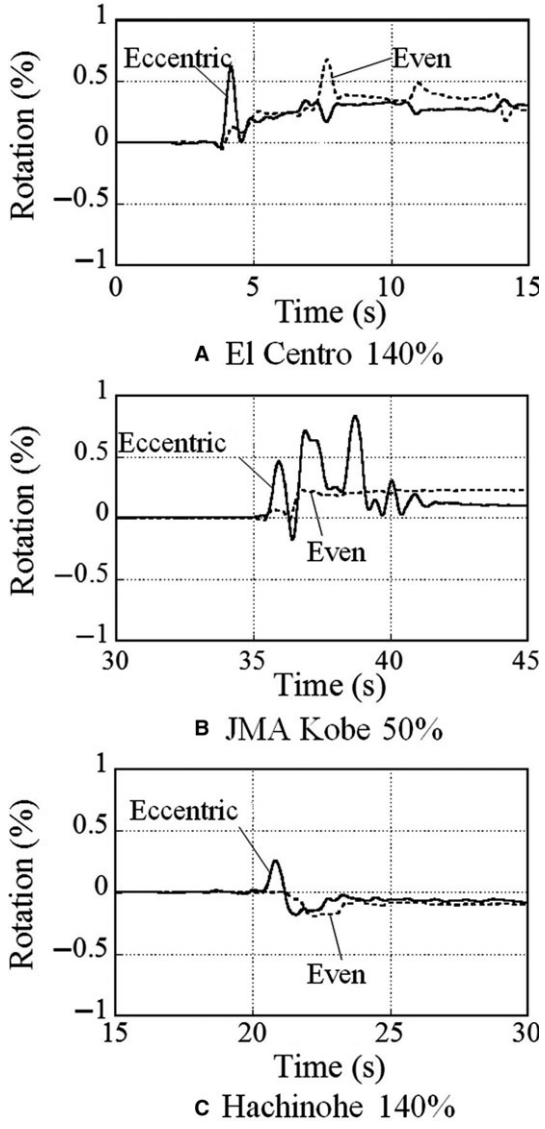

Figure 17. Twisting angle time histories

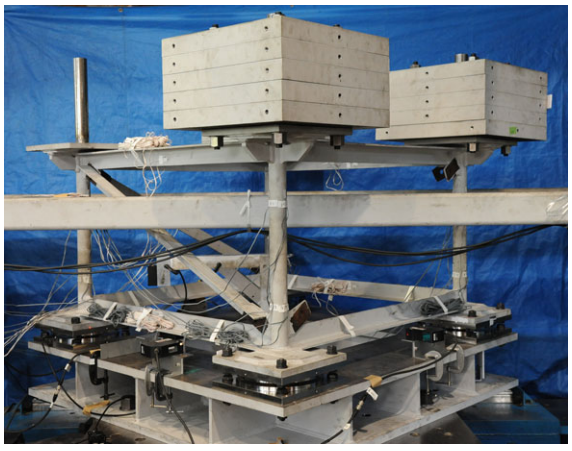

Figure 18. Setup of shake table test (uplift)

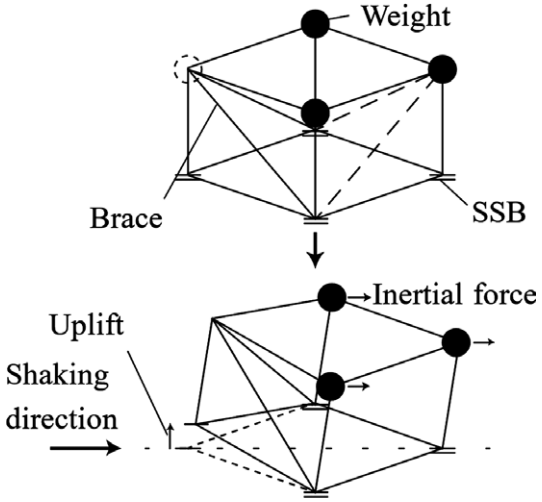

Figure 19. Uplift mode

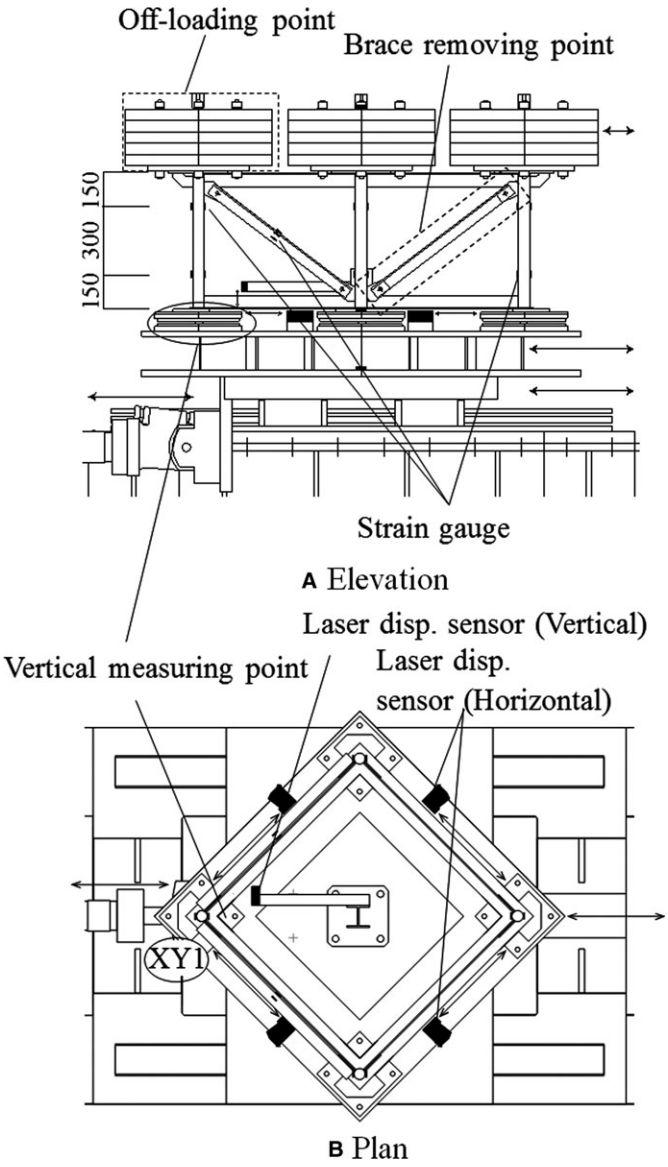

Figure 20. Measurement instrumentation

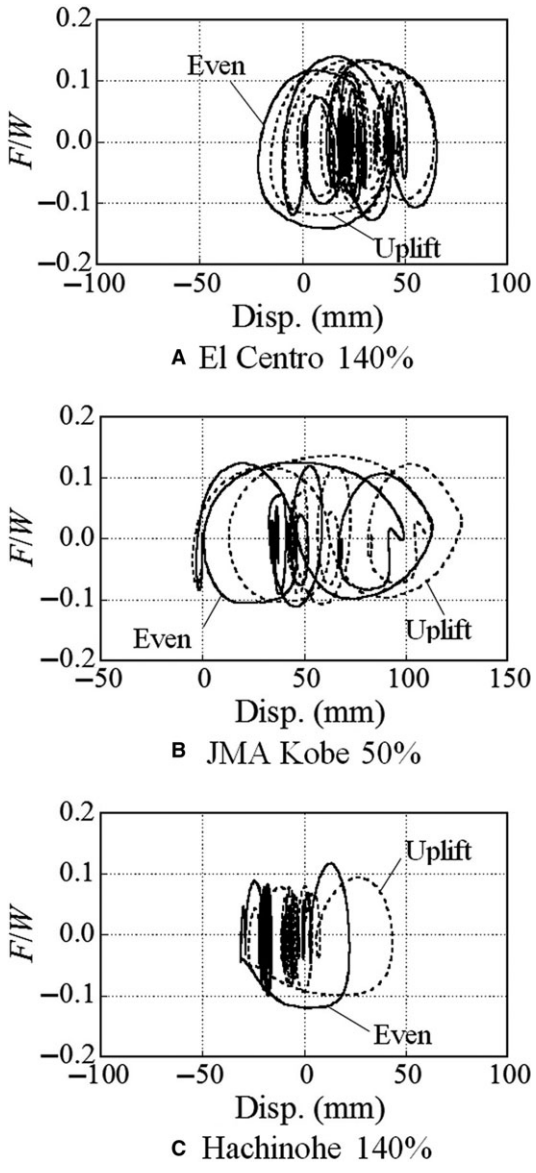

Figure 21. F/W–Horizontal displacement relationships

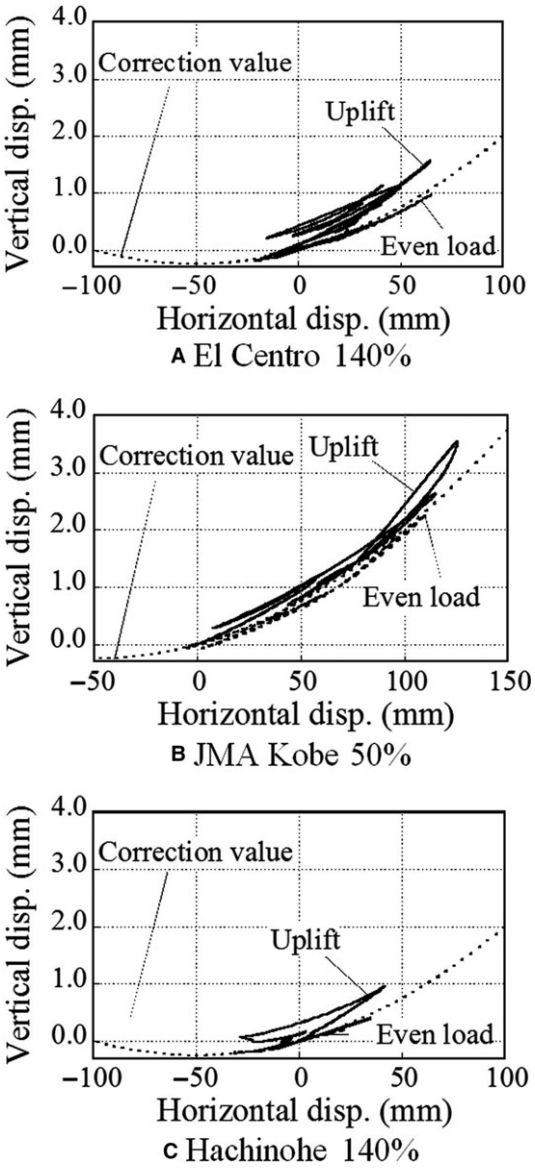

Figure 23. Vertical displacement orbits

$$\mu' = \mu_0 \times \left(1.746\sigma^{-0.141} + 0.02\right) \times \left(1 - 0.55e^{-0.019v}\right) \quad (4)$$

where μ' is the coefficient of friction, μ_0 is the reference friction coefficient (0.047), σ is the surface pressure acting on the slider, and v is the velocity at the top of the SSB.

The friction coefficient evaluation formula is identified based on the third cycle in the static tests in practical scale (600-mm diameter) and high-pressure (60 N/mm^2) specimens, which include the influence of temperature rise owing to frictional heat in the slider. The difference in the friction coefficient in these reduced-scale tests is mainly caused by lower surface pressure while the temperature can still affect because the slider is smaller than the real-size specimens.[11] Therefore, the friction coefficient can be expressed using three parameters: surface pressure, velocity, and temperature. However, the effect of temperature is difficult to express in simple form because it is considered a complex function of the slider

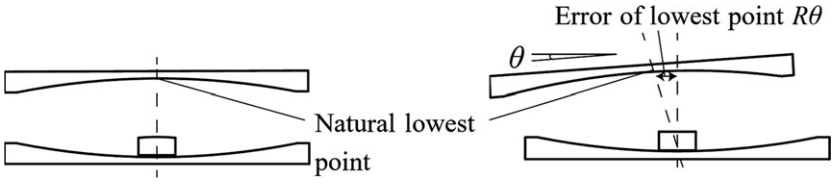

Figure 22. Schematic of lowest point error

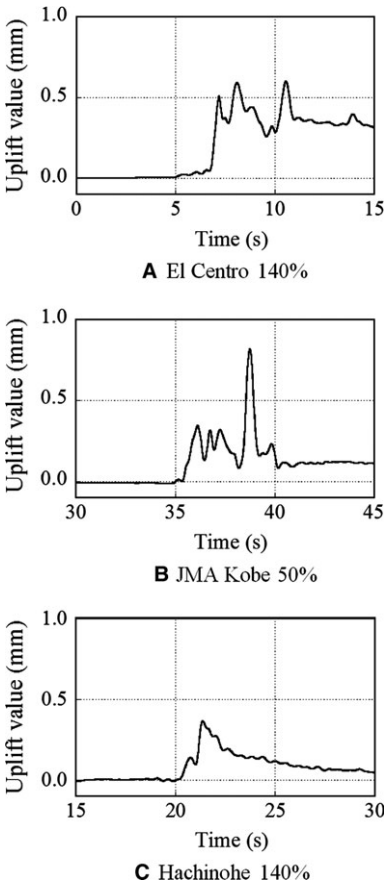

Figure 24. Assumed uplift time history

diameter, relative velocity, and cumulative displacement. Under such conditions, the abovementioned effect is recursively identified as a function of the pressure and velocity, which is expressed by the correction function of Equation (5). The friction coefficient is expressed by Equation (6).

$$\alpha_L = e^{\left(20+v^{0.4}\right)/\sigma^2} \tag{5}$$

$$\mu(\sigma, v) = \mu_0 \times \left(1.746\sigma^{-0.141} + 0.02\right) \times \left(1 - 0.55e^{-0.019v}\right) \times e^{(20+v^{0.4})/\sigma^2} \leq 0.16 \tag{6}$$

Figures 26 and 27 show plots of the equivalent friction coefficient and velocity and surface pressure relationship shown in Figures 8 and 9, respectively, compared with the values obtained from Equation (6). The result of Equation (6) corresponds well with the experimental value. As described earlier, a PTFE-based friction material possesses a friction coefficient that depends on the velocity. To reflect this characteristic in the dynamic model, we change the friction coefficient according to the velocity of the elasto-plastic model or express the effects of the velocity dependence by combining the elasto-plastic and viscous elements. Although the first method was often employed in past studies, we try to express the velocity dependence using the second method and confirm its validity here. In detail, Figures 28 and 29 show that friction coefficient

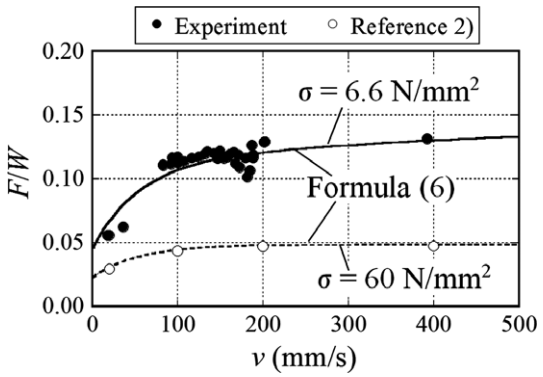

Figure 26. F/W–velocity relationships

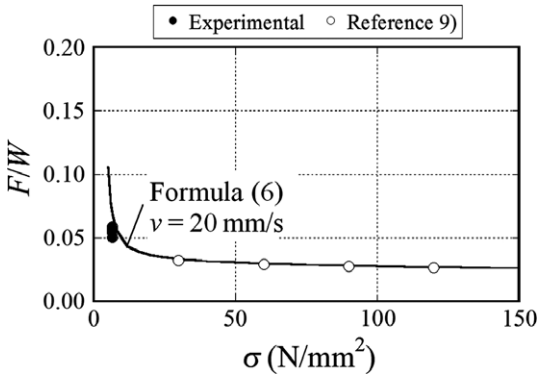

Figure 27. F/W–pressure relationships

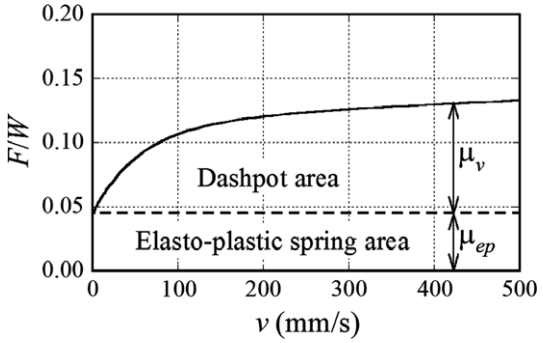

Figure 28. F/W–v relationship of SSB model (pressure 6.6 N/mm²)

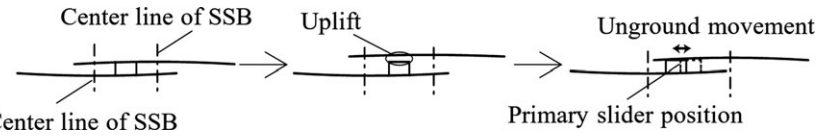

Figure 25. Schematic of ungrounded movement along uplift

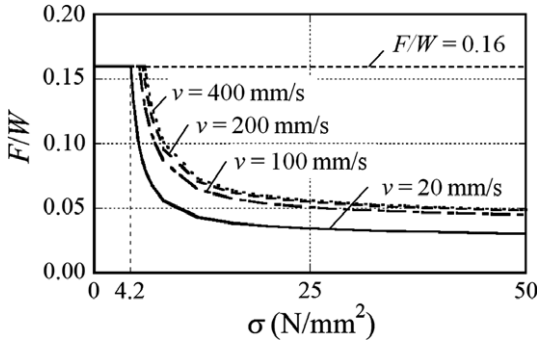

Figure 29. F/W–pressure relationship of SSB model

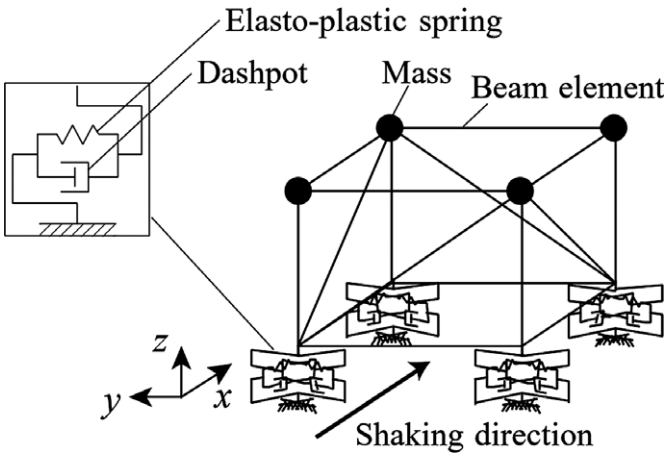

Figure 30. Analysis model

$\mu(\sigma, v)$, expressed in Equation (6), is divided into an elasto-plastic element (function of σ) and viscous element (function of v). The bilinear elasto-plastic element with a yield strength of $\mu_{ep}(\sigma)$ (expressed by Equation 7) is set, and secondary stiffness K is set at a secondary natural period of 4.5 seconds. The viscous element is set as $\mu_v(v)$ (expressed by Equation 8) as approximated by the tri-linear curve along the velocity. Please note that the effect of the bidirectional response or surface pressure changes owing to the vertical response is not considered in the proposed model.

$$\mu_{ep}(\sigma) = \mu_0 \times \left(1.746\sigma^{-0.141} + 0.02\right) \times 0.45 \times e^{20/\sigma^2} \quad (7)$$

$$\mu_v(v) = \mu - \mu_{ep} \quad (8)$$

4.2 Simulation of test results

By using the proposed dynamic model, a time-history analysis that reproduces the shake table tests presented in Section 3 is carried out. Figure 30 shows the analysis model. Table 3 lists the pressure conditions at the bearings in the evenly distributed loading tests and the loaded and unloaded pressure in the eccentric-loading tests. Newmark-β method are used for time-integration with incremental time of 0.01 seconds and damping factor of 0.02 for the upper structure. The variation in the response-axial force is neglected in analyses in this manuscript.

Table 3. Assumed pressure in analysis model

	σ (N/mm²)
Even load	6.6
Eccentricity	
Heavy	4.3
Light	1.9

The obtained time histories of displacements and accelerations in each seismic wave are shown in Figures 31 and 32, respectively, compared with the test results. All of the results generally show good agreement. In particular, the acceleration displays high accuracy. Good correspondence is also obtained for the eccentric-loading tests. Figure 33 shows the equivalent friction coefficient – displacement relationship using the evenly distributed weight tests. Although a difference of approximately 30% exists in the maximum response displacement in the JMA Kobe pulse wave, the experimental values obtained from the other seismic wave input are well simulated by the proposed model. Figure 34 shows the eccentric loading tests results compared with the analysis results. Even when the surface pressure condition in each bearing is varied, the proposed dynamic model exhibits a response that is

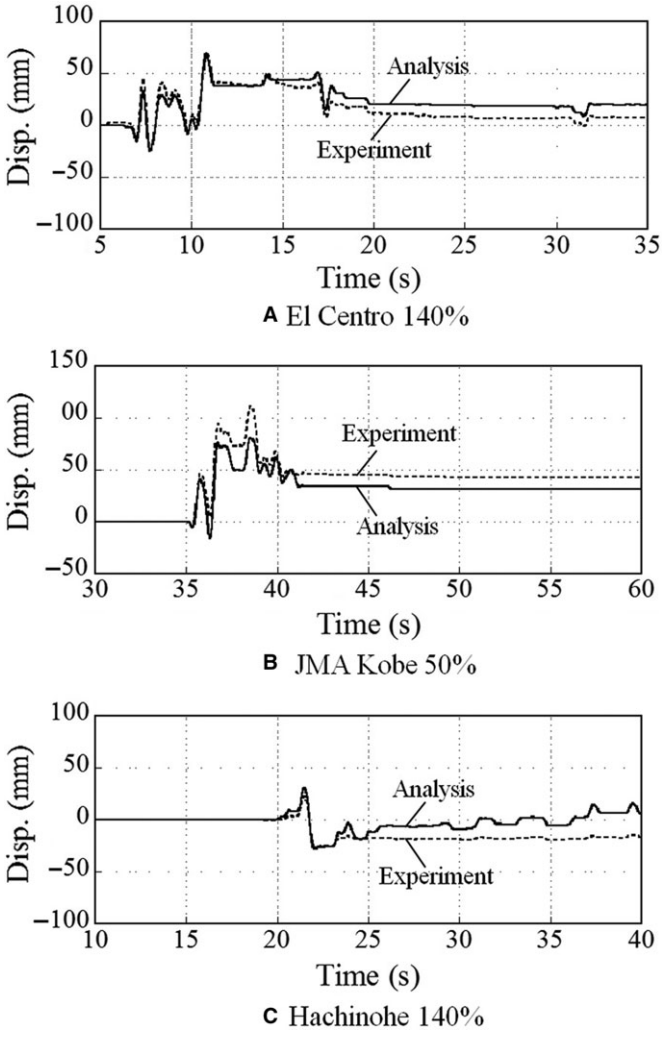

Figure 31. Time history of displacement response

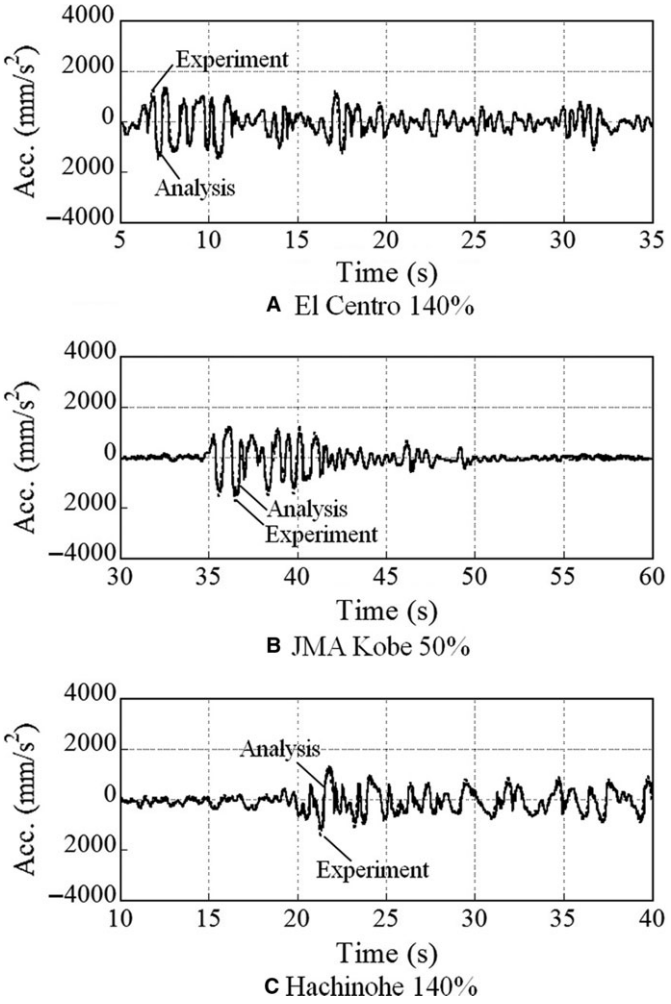

Figure 32. Time history of acceleration response

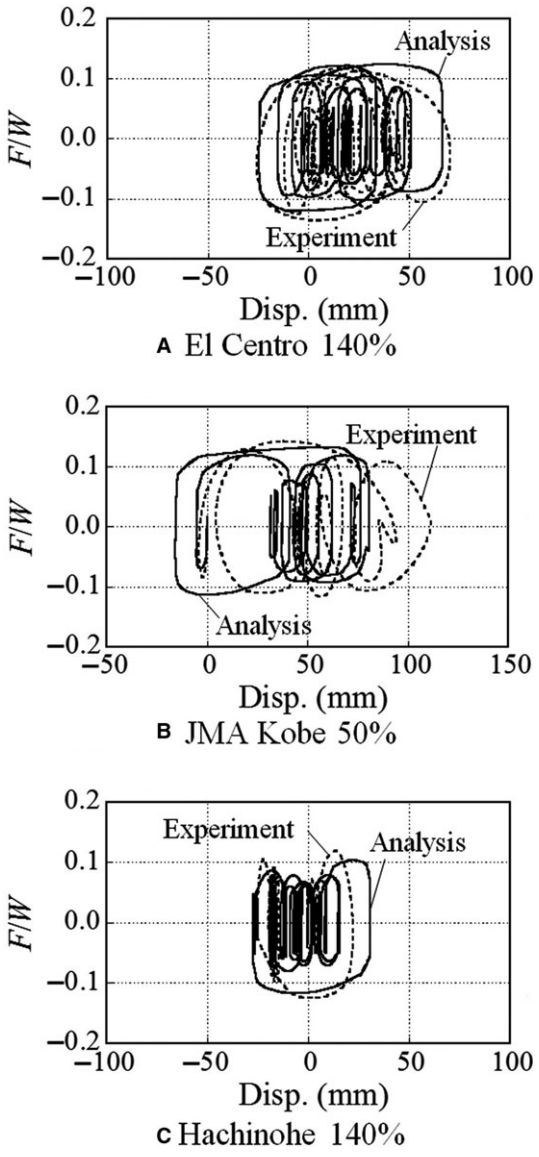

Figure 33. F/W–horizontal displacement relationship (evenly distributed)

well-compatible with the test results. Other cases exhibited similar tendencies.

From the abovementioned results, the proposed dynamic model is considered to be valid in modeling the dynamic response of the SSB. Although the above comparison is carried out under low-pressure shake table tests, we consider that the velocity dependence and influence of the viscosity part decrease as the surface pressure increases.

5. Conclusion

In this research, we conducted shake table tests of a frame supported by SSBs that include load eccentricity and uplifting conditions and investigated their response characteristics. From the results, an SSB dynamic model that considers the velocity dependence was proposed, and we confirm its validity by comparing the test results. The findings are summarized as follows.

1. In the experiment, we confirmed that the friction coefficient under low pressure of approximately 1/10 times the reference surface pressure increased by approximately double the standard value of the high surface pressure. The friction coefficient also increased because the velocity was found to be more prominent.
2. The maximum torsional response value under eccentric loading conditions exhibited no determinate difference from those under evenly loaded conditions. Amplification of the torsional response was also insignificant.
3. Under uplifting conditions, free running of the slider was observed, and the residual vertical displacement tended to remain. However, the influence on the horizontal response was insignificant.
4. The effects of low pressure and temperature on the friction coefficient were expressed by the functions of the pressure and velocity, and the proposed dynamic model composed of elasto-plastic and viscous elements was confirmed to be valid for evaluating the current test results and Ref. 9).

Acknowledgements

The authors express their sincere thanks to Mr. Hisami Hasegawa of Nippon Steel Sumikin Engineering Co., Ltd. and to Mr. Hideo Inoue and Mr. Nishio Mori of Daifuku Co., Ltd., for their valuable suggestions.

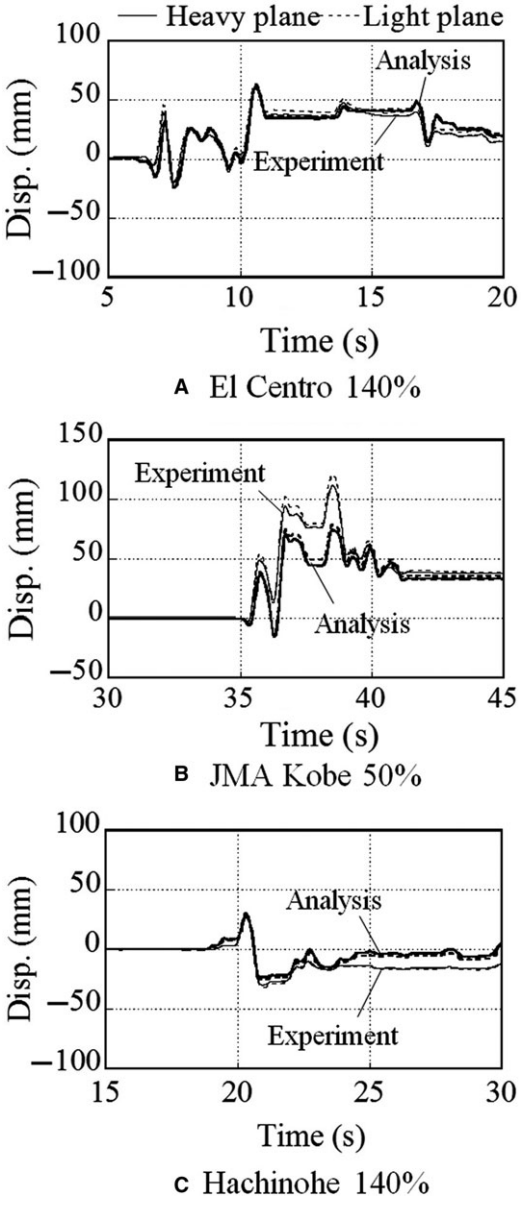

Figure 34. Time history of the displacement response (eccentric)

Disclosure

The authors have no conflicts of interest to declare.

References

1 Mokha A, Constantinou MC, Reinhorn AM, Zayas VA. Experimental study of friction-pendulum isolation system. Journal of Structural Engineering, ASCE, Vol. 117, No. 4, pp. 1201–1217, 1991.
2 Fenz DM, Constantinou MC. Behavior of the double concave friction pendulum bearing. Earthquake Engineering and Structural Dynamics, No. 35, pp. 1403–1424, 2006.
3 Constantinou M, Whittaker AS, Velivasakis E. Seismic evaluation and retrofit of the Ataturk international airport terminal building. Research Progress and Accomplishments: 2000-2001, MCEER Bulletin.
4 Mokha AS, Lee PL, Wang X, Yu P. Seismic isolation design of the new international terminal at San Francisco international airport. Conf. Struct. Eng. In the 21st Century, 1999.
5 Li T, Shimoda K, Osada O. Concept test of bearing materials for use in friction pendulum seismic isolators. Summaries of Technical Papers of Annual Meeting Architectural Institute of Japan, Structure I, pp. 609–610, 1991.8 (in Japanese)
6 Ono H, Ino S, Takagi K, Koyama M, Nakao F. Study of dynamic behavior of a nuclear power plant with sliding isolation pendulum bearings. Summaries of Technical Papers of Annual Meeting Architectural Institute of Japan, Structure II, pp. 1259–1260, 2012 (in Japanese).
7 Koibuchi T, Saito K, Kurita S, Chiba D. Restoring force characteristic at lower slip velocities of FPS based on seismic response records. Proceedings of AIJ Tohoku Conference, Structure (68), pp. 105–108, 2005 (in Japanese).
8 Constantinou MC, Mokha A, Reinborn A. Teflon bearings in base isolation II: modeling. Journal of Structural Engineering, ASCE, Vol. 116, No. 2, pp. 455–474, 1990.
9 Nakamura H, Nishimoto K, Tomimoto A. Development of spherical sliding bearing. Nippon Steel & Sumikin Engineering Technical Review, Vol. 6, pp. 28–35, 2015 (in Japanese).
10 Kawashima K. A computational model of friction force in dynamic response analysis. Journal of Japan Society of Civil Engineering, No. 309, pp. 151–154, 1981 (in Japanese).
11 Takahashi Y, Hibi M, Iemura H. Numerical model of frictional isolator considering multi-dependencies. Journal of Applied Mechanics, Vol. 8, pp. 701–708, 2005 (in Japanese).

How to cite this article: Takeuchi T, Nakamura H, Uchida M, Yoshida M, Matsui R. Shaking table tests on spherical sliding bearings taking eccentricity and uplift into account. *Jpn Archit Rev.* 2019;2:172–184. https://doi.org/10.1002/2475-8876.12080